Water dynamics at the solid-liquid interface to unveil the textural features of synthetic nanosponges.

Journal:	*Journal of the American Chemical Society*
Manuscript ID	ja-2019-13435c
Manuscript Type:	Article
Date Submitted by the Author:	13-Dec-2019
Complete List of Authors:	Lo Meo, Paolo; Universita degli Studi di Palermo, STEBICEF Mundo, Federico; Universita degli Studi di Palermo, STEBICEF Terranova, Samuele; Universita degli Studi di Palermo, STEBICEF Conte, Pellegrino; Universita degli Studi di Palermo, Dipartimento di Scienze Agrarie e Forestali Chillura Martino, Delia; Universita degli Studi di Palermo,

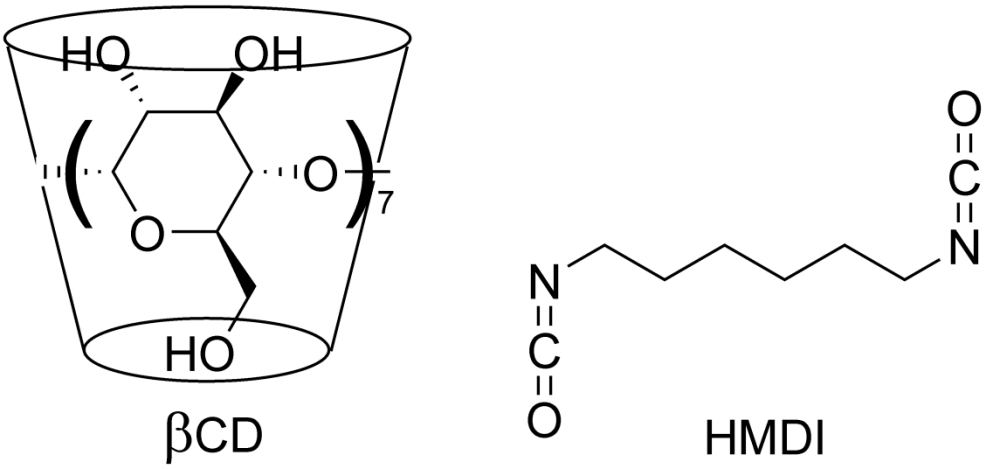

Figure 1. Structures of βCD and HMDI.

73x35mm (1200 x 1200 DPI)

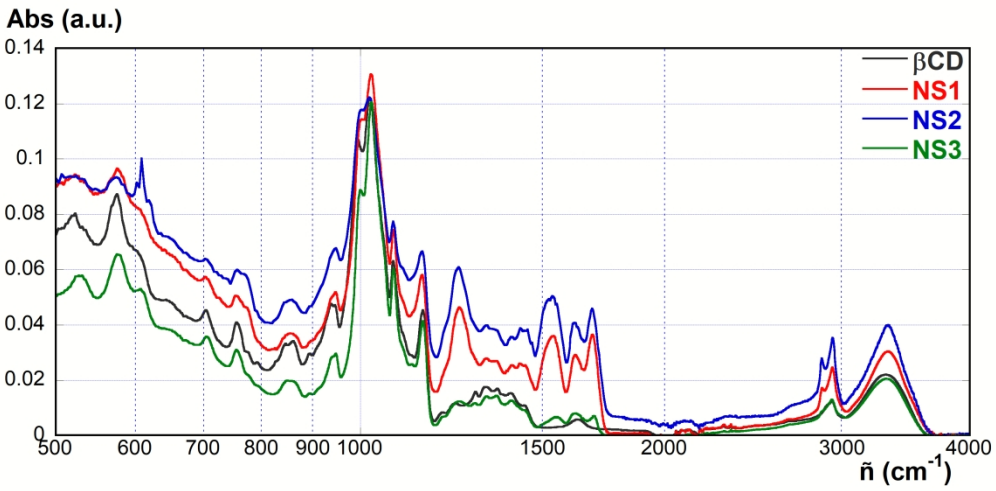

Figure 2. ATR-FT-IR spectra of βCD and NS1, NS2, NS3.

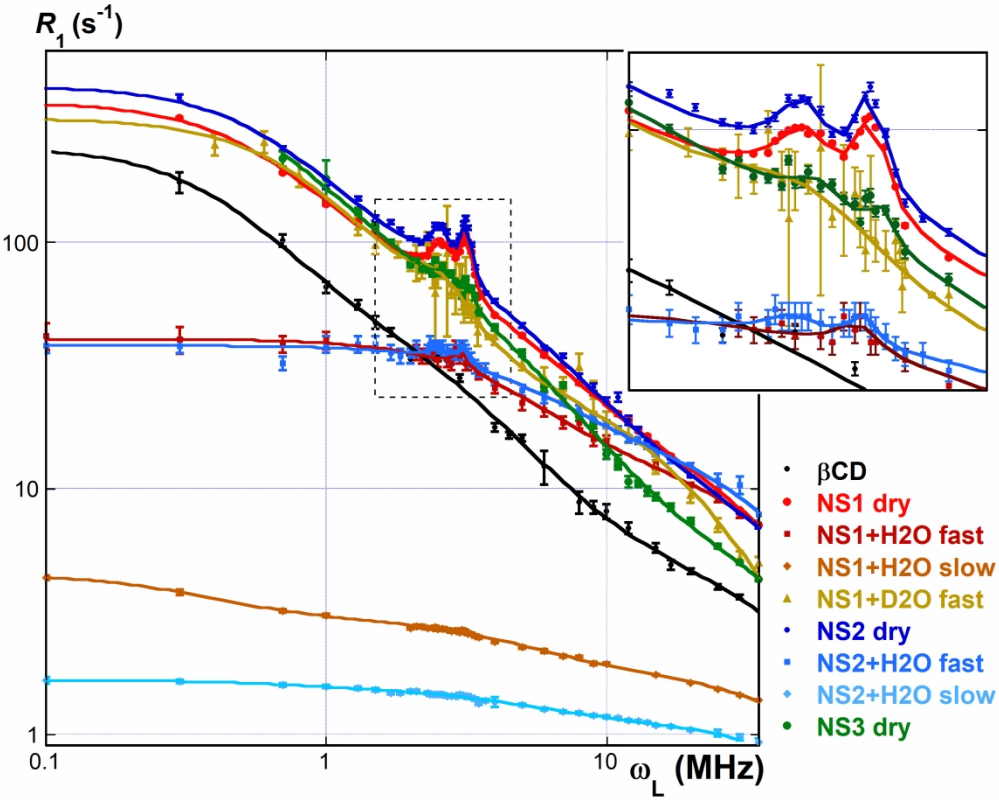

Figure 3. NMR dispersion curves (R_1 vs ω_L).

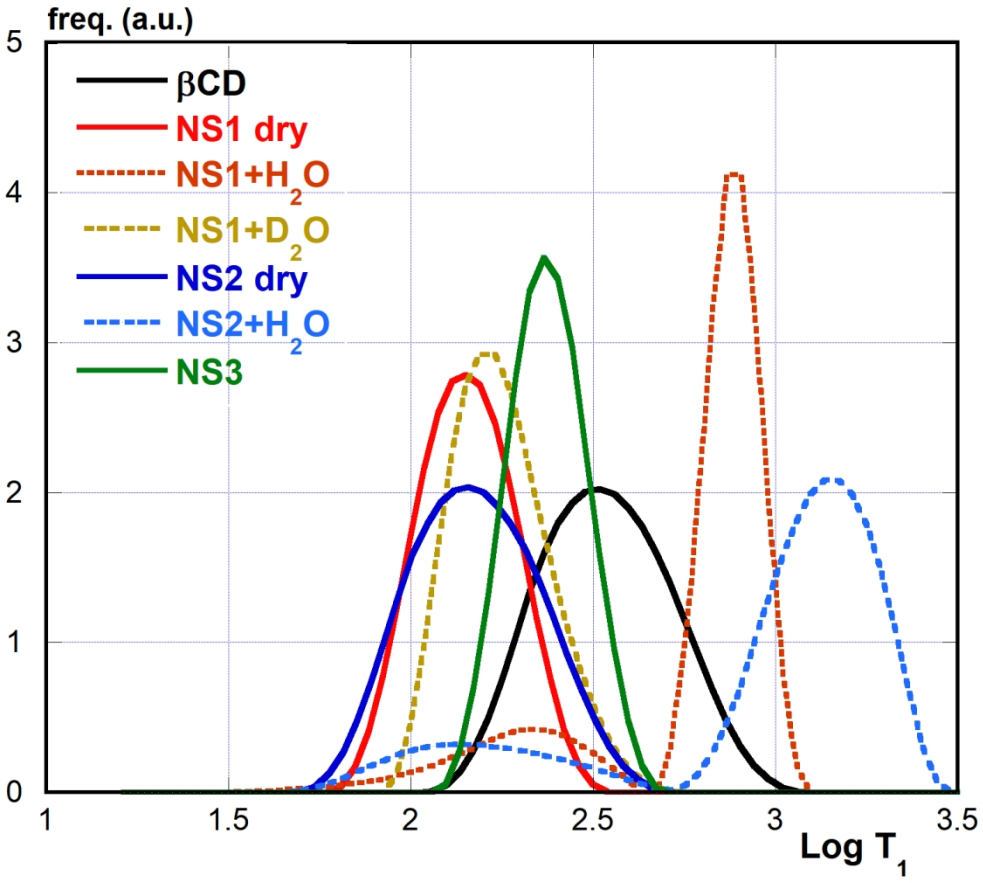

Figure 4. Normalized Inverse-Laplace transforms (UPEN) at 35 MHz.

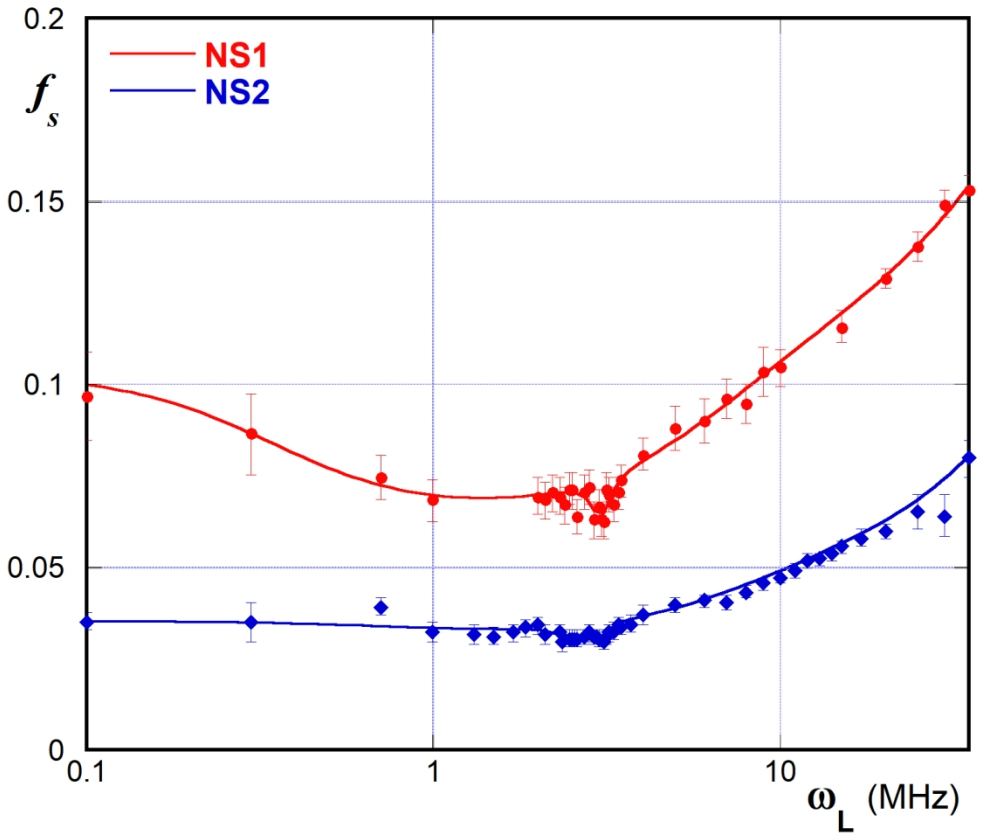

Figure 5. Apparent dependence of f_s on ω_L for NS1 and NS2.

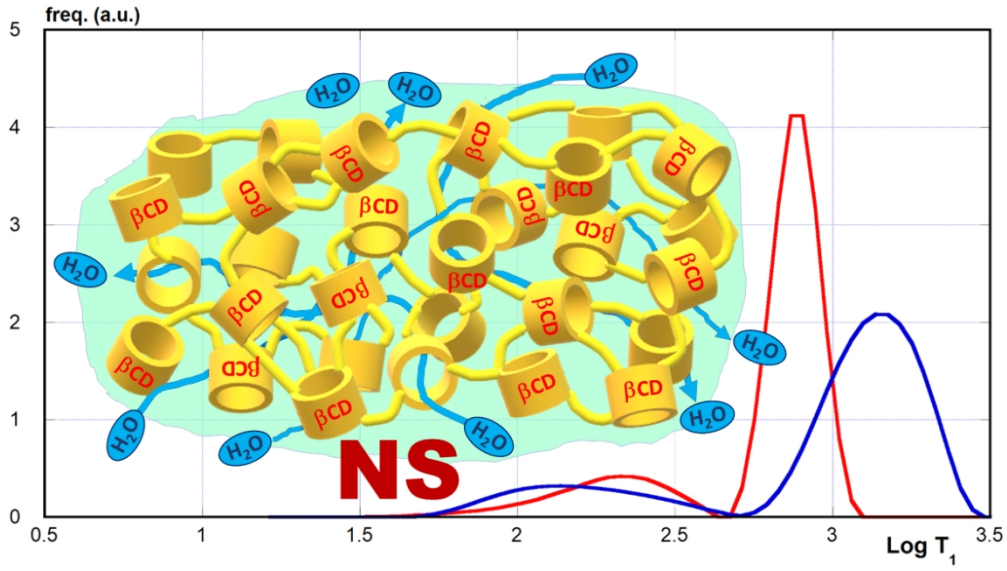

TOC Graphics

309x175mm (96 x 96 DPI)

Water dynamics at the solid-liquid interface to unveil the textural features of synthetic nanosponges.

Paolo Lo Meo,*† Federico Mundo,† Samuele Terranova,† Pellegrino Conte,*‡ Delia Chillura Martino.†

† Dept. of Biological, Chemical and Pharmaceutical Sciences and Technologies (STEBICEF), University of Palermo; V.le delle Scienze ed. 17, 90128 Palermo, Italy.

‡ Dept. of Agricoltural, Food and Forest Sciences (SAAF), University of Palermo; V.le delle Scienze ed. 4, 90128 Palermo, Italy.

KEYWORDS Connectivity, Cyclodextrins, FFC-NMR Relaxometry, Nanosponges, Porosimetry.

ABSTRACT: A Fast-Field-Cycling NMR investigation was carried out on a set of polyurethane cyclodextrin nanosponges, in order to gain information on their textural properties, which have been proven to be quite difficult to assess by means of ordinary porosimetric techniques. Experiments were performed on both dry and wet samples, in order to evaluate the behavior of the "non-exchangeable" C-bound ^{1}H nuclei, as well as the one of the mobile protons belonging to the skeletal hydroxyl groups and the water molecules. The results acquired for the wet samples accounted for the molecular mobility of water molecules within the channels of the nanosponge network, leading back to the possible pore size distribution. Owing to the intrinsic difficulties involved in a quantitative assessment of the textural properties, in the present study we alternatively propose an extension to nanosponges of the concept of "connectivity", which has been already employed to discuss the properties of soils.

INTRODUCTION

Nanosponges (NSs)[1-3] are an emerging class of smart materials. Their tunable absorption and release abilities towards both organic[4] and inorganic[5] species make them ideal candidates as platforms for drug carrier/delivery systems,[6-7] environmental remediation devices[8-9] and supports for metal nanoparticle catalysts.[10-13] These materials are obtained by reacting supramolecular host units (e.g. cyclodextrins,[14] calixarenes,[15] pillararenes[16]) with suitable reticulating agents that afford the linker units. The properties of NSs can be widely tuned by either pre-modification of the host monomers or post-synthesis chemical modification of the obtained product.[17] Moreover, reticulating agents bearing ionizable (polyamines,[18] triazoles,[19] pyromellytic anhydride[20-21]) or other stimuli-sensitive[22] groups can be used; hence, functional tailored materials can be obtained.

A reliable evaluation of the textural features, such as average pore size (D), specific surface area (S) and specific pore volume (V), constitutes one of the main issues in the characterization of NSs, in order to rationalize their properties. Because of their peculiar highly disordered structure, NSs are supposed to present a thick network of nanosized channels between the host monomers. However, it has been reported on several occasions that the ordinary methodologies based on the N_2 gas adsorption isotherms, analyzed by means of the well-known BET[23] and BJH[24] approaches, result in abnormally low values (sometimes even below the instrumental sensitivity limits), unless particularly long and rigid structural units are used as the linkers. For instance, S values ranging up to 263 $m^2 g^{-1}$ were claimed for a series of materials obtained from β-cyclodextrin (βCD) and tetrafluoro-terephtalonitrile.[25] Comparable results were found by using decafluorobiphenyl,[26] whereas an outstanding area of 1225 $m^2 g^{-1}$ and a pore volume of 1.71 $cm^3 g^{-1}$ were found for a material obtained by reacting a *per*-benzyloxy-cyclodextrin with formaldehyde dimethylacetal.[27] Nevertheless, beyond these few exceptions, S values by far below 10 $m^2 g^{-1}$ are usually found for materials prepared from cyclodextrins and typical reticulating agents such as diisocyanates,[28-29] epichlorohydrin,[30-31] or polycarboxylic acids.[32-33] Similarly, S values not larger than 8 $m^2 g^{-1}$ were found for a series of cyclodextrin-calixarene co-polymers, together with pore volumes smaller than 0.03 $cm^3 g^{-1}$ and average pore sizes smaller than 4 nm.[34] Wilson et al. recently examined a series of polyurethane βCD polymers obtained with diverse reticulating diisocyanates.[35] They studied the relevant textural properties by both the ordinary BET method and a different approach based on the absorption of a suitable probe dye, namely *p*-nitrophenol, having a known molecular area (0.525 nm^2) and volume (0.0908 nm^3). The latter methodology relies on the evaluation of the maximum absorption capacity of the material, obtained analyzing the absorption isotherms by either the Langmuir or the Sips model. It led to estimate S values in the order of several hundreds of $m^2 g^{-1}$, which undoubtedly appear a much more sensible result, in comparison to N_2 adsorption. However, even the *p*-nitrophenol method is not devoid of criticism (see later). In particular, the cited Authors explicitly state that "*the surface areas of the sorbents are probe dependent, and adsorbate parameters … may not be representative of binary solution conditions*"; moreover, "*differences in the adsorption parameters from the solid-gas vs. solid-solution isotherms were attributed to differences arising because of hydration and swelling … of the copolymer framework*" that may unpredictably provide structural microscopic rearrangements. [35] Therefore, it seems that the concept itself of "surface" has conceivably a somehow elusive or deceptive meaning in the case of NS materials, so that new paradigms should be possibly explored.

Since the seminal work by Brownstein and Tarr,[36-38] Fast-Field-Cycling (FFC) NMR relaxometry has been used as a valuable tool to assess water mobility at the liquid-solid interface (and also to study the microscopic dynamics of polymers[39-44] and proteins[45-48]). Data interpretation can be related to the textural features of solid systems such as clays and microporous materials in general.[49-59] Very briefly (the bases of FFC-NMR relaxometry are summarized in the Supporting Information), this technique relies on the simple though counterintuitive idea that the tighter a water molecule is bound to the surface of a porous wet system (that is the more restricted its motion is), the faster longitudinal relaxation rate (R_1) water ^{1}H nuclei will experience (the same is true, indeed, also for transverse relaxation, which we do not consider here). Thus, as long as water is trapped into micropores, mesopores or macropores, the observed R_1 values decrease in the same order.[60] Therefore, FFC-NMR relaxometry can also be used as a valid alternative to the traditional porosimetry investigations to obtain pore size distributions.[60] Very recently, FFC-NMR relaxometry has been also applied in soil science[61] to quantitatively measure the hydrological connectivity inside the soil (HCS).[62-63] In general, connectivity refers to the processes involving a transfer of matter, energy, and/or organisms within or between elements of an ecological system. This implies the presence of a transport vector, such as water.[62-63] More in detail, according to Conte and Ferro, "*hydrological connectivity inside the soil refers to how spatial patterns inside the soil (i.e., the structural connectivity) interact with physical and chemical processes (i.e., the functional connectivity) in order to determine the subsurface flow (i.e., the water transfer), thereby explaining how sediment transport due to surface runoff (i.e., the soil particle transfer) can be affected*".[62-63] Hence, the effects of heterogeneities of a complex and non-homogeneous physical system can be evaluated.

Due to the presence of channels and sinks in the structure of NSs, we reasoned that the concept of connectivity developed in ecology and soil science, might be also suitable for the description of these materials. In order to develop a different methodology for assessing their texture features, in the present work we performed an FFC-NMR study of three NS materials (referred to as NS1, NS2, and NS3) obtained by reacting β-cyclodextrin with hexamethylene-diisocyanate (HMDI, Figure 1).

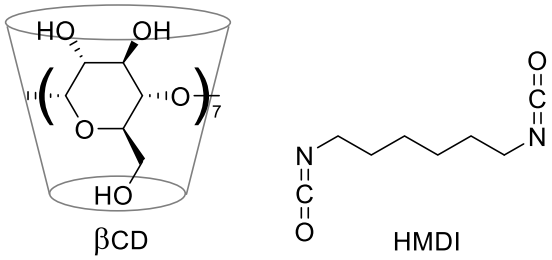

Figure 1. Structures of βCD and HMDI.

Different mole-to-mole ratios (i.e., 1:4, 1:2 and 1:1, respectively) were applied, in order to achieve a different extent of reticulation. The reaction between the -OH groups of βCD and the –N=C=O groups of HMDI results in the formation of urethane units. The relaxometric behavior of the nanosponges obtained was studied for both dry and wet samples, in order to consider the dynamics of water molecules into the nanochannels subjected to possible swelling.

RESULTS AND DISCUSSION

Synthesis and Characterization

Preparation of materials NS1, NS2 and NS3 was accomplished according to literature reports[35] (see Supporting Information for details). In brief, anhydrous βCD and HMDI were mixed in the proper mole-to-mole ratio, in the presence of a small amount of dry DMSO in order to ease reactants mixing. In the case of NS1 and NS2, the accomplishment of the reticulation process was immediately verified by the mechanical hardness and lack of solubility of the reaction products, which were recovered almost quantitatively. Conversely, NS3 resulted partly soluble in water, thereby providing a lesser reaction yield (ca. 70 %). The latter observation can be justified by the insufficient amount of HMDI, which prevented a full reticulation.

The formation of the polymeric network was confirmed by ATR-FTIR analysis (spectra are synoptically shown in Figure 2).

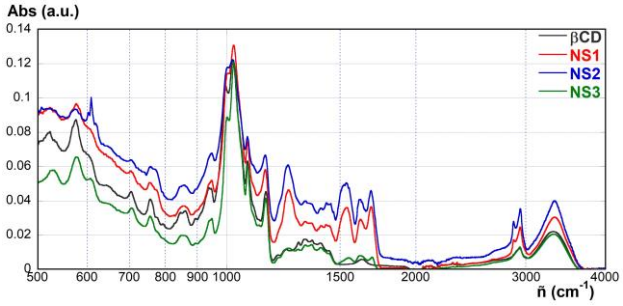

Figure 2. ATR-FT-IR spectra of βCD and NS1, NS2, NS3.

The main features in the spectrum of the starting βCD are the large O-H str. band centered at 3304 cm^{-1}, followed by a tiny C-H str. signal at 2918 cm^{-1} and by the typical βCD fingerprints system (various C-O str.) in the range 1200~900 cm^{-1}. NS1 and NS2 spectra show three main additional features: *i*) two signals in the C-H stretching region between 2926 and 2859 cm^{-1}, accounting for the presence of methylene groups in the linker bridges; *ii*) a system of three signals at 1694, 1630 (amide-I-like carbonyl str.), and 1548 cm^{-1} (amide-II-like N-H bend.), accounting for the presence of the urethane groups formed during the reticulation; *iii*) a strong signal at 1251 cm^{-1}, conceivably due to the O-carbonyl str. of the urethane groups. The same signals, though much weaker, were also identified in the spectrum of NS3. Noticeably, no trace of a possible signal around 2268 cm^{-1} (-N=C=O str.) was envisaged in the spectra, thereby ruling out the presence of unreacted reticulating agent.

Porosimetry

Porosimetric determinations (i.e., N_2 absorption isotherms) performed on the fully insoluble materials NS1 and NS2 afforded, as expected, very poor results, partly beyond the lower sensitivity limit of

the applied instrumental apparatus. In particular, by means of the BET analysis, an S value of 0.134 $m^2 g^{-1}$ for NS2 was found only. The use of the BJH analysis resulted in S values of 0.115 and 0.280 $m^2 g^{-1}$ for NS1 and NS2, respectively. This trend follows the reticulation degree expected on the grounds of the amount of reticulating agent used in the syntheses. A V value of 0.001 $cm^3 g^{-1}$ was found for both NS1 and NS2, with an average pore diameter of 7.1 and 3.8 nm for the two systems, respectively. The latter finding does not appear consistent with the expected reticulation degree. On the whole, these results agree with those reported elsewhere,[35] thereby confirming that N_2 absorption is not a suitable method for the measurement of nanosponge textures.

We also evaluated the specific surface areas and volumes of NS1 and NS2 by means of the *p*-nitrophenol absorption method. Absorption isotherms were studied at 25 °C in aqueous acetate buffer at pH 4.4. Data were subjected to regression analysis by means of the Sips equation in the form: $q_e = q_{max} \cdot (K \cdot c_{eq})^n / [1+(K \cdot c_{eq})^n]$, where q_e and q_{max} are the amount of guest absorbed at equilibrium and the maximum capacity of the material ($mol\,g^{-1}$) respectively, c_{eq} is the concentration of the guest at equilibrium, K is the apparent equilibrium constant and n is an empirical coefficient. We found for NS1: $q_{max} = (7.8 \pm 0.6) \cdot 10^{-4}$ mol g^{-1}, $K = (2.1 \pm 0.2) \cdot 10^3$ M^{-1}, $n = 1.36 \pm 0.08$; for NS2: $q_{max} = (7.9 \pm 0.9) \cdot 10^{-4}$ mol g^{-1}, $K = (1.74 \pm 0.06) \cdot 10^3$ M^{-1}, $n = 1.21 \pm 0.09$. As a consequence, very similar apparent S (250 ± 30 $m^2 g^{-1}$) and V (0.043 ± 0.004 $cm^3 g^{-1}$) values can be estimated for both materials. These results are comparable with those reported by Wilson et al.[35] for a material with the same composition as NS2 (i.e., $q_{max} = 11.5 \cdot 10^{-4}$ mol g^{-1}, $S = 364$ $m^2 g^{-1}$). The discrepancy between the q_{max} values is likely due to the presence of the buffer, according to the well-known effect of electrolytes on the binding equilibria of free cyclodextrins in solution.[64-66]

The previous results can be interestingly compared with the composition of NS1 and NS2, which contain $5.5 \cdot 10^{-4}$ and $6.8 \cdot 10^{-4}$ mol g^{-1} of βCD, respectively. In general, *p*-substituted nitrobenzene derivatives form in solution only 1:1 complexes both with native and chemically modified βCDs;[67-70] however, due to the smaller volume of these guests as compared to the host cavity, a simultaneous dynamic co-inclusion of solvent molecules occurs.[70] Moreover, evidence has been reported (2D-LFSE solid-state NMR) that in the case of the inclusion of a *p*-nitroaniline derivative in a polyamino-cyclodextrin NS, the guest specifically occupies the cyclodextrin cavities and does not resides into the nanochannels.[18] Now, the q_{max} values found experimentally suggest that most of the *p*-nitrophenol guest should be included into the host cavities, whereas only a minor amount (i.e., ca. 30% for NS1, ca. 14% for NS2) may reside into the nanochannels. This implies that the channels surface, which represents the interspace between the cyclodextrin units, is not adequately sampled. Furthermore, taking into account the intrinsic volume of the βCD cavity (i.e. 0.262 nm^3, which corresponds to 15.77 cm^3 mol^{-1} or 0.14 cm^3 g^{-1}), from the composition of NS1 and NS2, one can calculate that, even neglecting the contribution from nanochannels, minimum V values as large as 0.087 and 0.107 cm^3 g^{-1}, respectively, should be expected. The latter values are much larger than the experimental results. Thus, we can conclude that the use of the *p*-nitrophenol as a probe actually leads to underestimate both S and V values. Therefore, even the reliability of this approach appears seriously questionable.

FFC-NMR Relaxometry

Relaxometry experiments performed here aimed at studying the variations of the longitudinal relaxation rates (R_1) in the magnetic field range 0.1-35 MHz. We first investigated the dry NS1-NS3 samples; anhydrous βCD was also analyzed as a useful comparison. Then, we considered the two fully insoluble materials, NS1 and NS2 after equilibration with water, added in a 1:2 w/w amount (the relevant samples are indicated hereinafter as NS1+H_2O and NS2+H_2O). Hence, information on the dynamics at the solid-liquid interface was achieved. Finally, the dynamics of the skeletal ^1H nuclei was also studied by equilibrating NS1 with D_2O (1:2.5 w/w, sample NS1+D_2O). As a general remark, for the dry samples (βCD, NS1, NS2, NS3) ^1H relaxation followed a simple first-order exponential trend. Conversely, relaxation of the wet samples (i.e., NS1+H_2O, NS1+D_2O, NS2+H_2O) showed a more complex kinetic profile, which was suitably modeled as the sum of two distinct first-order processes: a "fast" and a "slow" one. This peculiar behavior is mirrored by the Inverse-Laplace transform analysis of the relaxation kinetic curves (see later). For the sake of completeness, we must mention here that for the NS1+D_2O sample the slow component was affected by very large errors, thereby showing a very scattered trend with respect to the proton Larmor frequency (ω_L); therefore, it was not further analyzed. NMR dispersion curves (R_1 vs ω_L) for all the samples are synoptically shown in Figure 3 (the complete dataset is reported in the Supporting Information, Table S1).

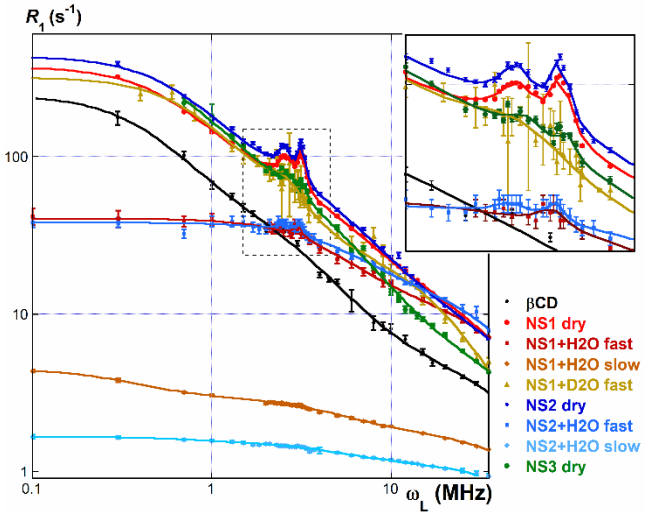

Figure 3. NMR dispersion curves (R_1 vs ω_L).

Interestingly, most of the dispersion curves show the presence of the typical dips located at ω_L ca. 2.7 and 3.1 MHz, due to the quadrupolar coupling effect with the urethane N atoms (inset in Figure 3). Dips are well detectable not only in the curves relevant to dry materials NS1, NS2 and NS3, but also for the fast components of the

NS1+H_2O and NS2+H_2O samples. The latter finding suggests the occurrence of strong long-range N-H interactions even under conditions able to favor proton exchange. Conversely, dips are absent in the dispersion curves relevant to the slow component of the wet samples, to the fast component of NS1+D_2O and, obviously, to dry βCD.

NMR dispersion curves were subjected to regression analysis according to Halle's approach,[71-73] as the sum of two or three "stretched" components, to which two additional Lorentzian-like contributions were added in order to account for the simultaneous occurrence of the quadrupolar dips (when needed):

$$R_1 = \sum_i \frac{c_i \tau_i}{1+(\omega_L \tau_i)^2} + \sum_{j(dips)} \left[\frac{2}{\pi} \cdot \frac{c_j s_j}{4(\omega_L - \omega_j)^2 + s_j^2} \right] \quad (1)$$

From the fitting parameters (reported in the Supporting Information, Table S2) the relevant correlation times (τ_c) for each curve were calculated (Table 1), according to the relationship:

$$\tau_c = \frac{\sum_i c_i \tau_i}{\sum_i c_i} \quad (2)$$

Table 1. Correlation times (τ_c).

Sample	τ_c (ns)	Sample	τ_c (ns)
βCD dry	600 ± 180		
NS1 dry	430 ± 40	NS2 dry	450 ± 50
NS1+H_2O fast	68 ± 5	NS2+H_2O fast	58 ± 4
NS1+H_2O slow	37 ± 4	NS2+H_2O slow	20 ± 4
NS1+D_2O fast	500 ± 90	NS3 dry	580 ± 240

For molecular compounds, τ_c is interpreted as the average time needed for a molecule to rotate one radian or to move within a distance equal to its length. Therefore, it can be considered as a suitable measure for structural mobility at a microscopic scale. Dry samples showed similar correlation times, within the limits of experimental uncertainties. By contrast, wet samples NS1+H_2O and NS2+H_2O showed much smaller τ_c values for the fast component, and even smaller values for the slow one. Both correlation times for NS1+H_2O are significantly larger than those for NS2+H_2O. Noticeably, sample NS1+D_2O shows a comparable τ_c value with respect to the relevant dry material. These observations suggest that correlation times for samples with H_2O mainly keep into account the relaxometric behavior of water molecules. However, we can distinguish at least two different populations having a significantly different mobility. Trends for τ_c values are consistent with the different reticulation degree expected for the materials. In fact, NS1 is supposed to present significantly narrower channels than NS2, having been prepared with a larger amount of reticulating agent. Therefore, we may reasonably relate the fast component (longer τ_c) of the relaxation kinetics to H_2O molecules which are tightly bound to the nanosponge network, thereby forming its immediate hydration shell/layer. This idea is supported by the residual presence of the quadrupolar dips observed in the relevant dispersion curve. Conversely, the slow component (shorter τ_c) may be associated to loosely bound molecules flowing within the lumen of the channels. At this purpose, it is worth mentioning here that dry materials retain a small percentage of water, ca. 5~7 % (by TGA analysis). On the grounds of trivial stoichiometric calculations, this averagely corresponds to 7 ± 2 water molecules per βCD unit. It is quite reasonable to assume that these water molecules are very tightly bound to the structure either via hydrogen bonding, or as small clusters placed inside the βCD cavities. Moreover, it can be estimated that nearly 75 % of the H atoms present in the samples are stably bound to C atoms, whereas the remaining 25 % are "exchangeable protons" bound to O or N atoms. Differently, for both the wet samples NS1+H_2O and NS2+H_2O it can be calculated that the exchangeable protons correspond to ca. 79% of the total H atoms population.

Close inspection of the dispersion curves tells a more articulated story. Seen on a logarithmic scale, curves for dry NS1 and NS2 appear almost superimposable at large ω_L values and only slightly diverging at low ω_L. This suggests that relaxation mechanisms are very similar in the two cases. However, relaxation for anhydrous βCD is much slower in the whole ω_L range, clearly indicating that lack of reticulation favors molecular motions on a microscopic scale. The curves for dry NS3 and NS1+D_2O are in intermediate position between βCD and dry NS1 at large ω_L, while they approach the latter ones at low ω_L values. This suggests an intermediate structural mobility. In the former case, this can be justified with the incomplete reticulation due to the low combination ratio between βCD and HMDI (i.e. 1:1 mole-to-mole), whereas, in the latter case, it positively indicates swelling occurrence. On passing to wet samples, curves for the fast component of NS1+H_2O and NS2+H_2O approach those for the corresponding dry materials only at the largest ω_L values, but neatly diverge in the region at low ω_L, where the relaxation rates for both samples are very similar and almost independent on the Larmor frequency. This peculiar behavior suggests that different sections of the dispersion curves account for different aspects of the microscopic dynamism of the samples. In particular, curve trends suggest that the relaxometric response appears more sensitive to not-exchangeable C-bound protons and to tightly bound water molecules of the hydration layer at the larger ω_L values. Conversely, larger sensitivity to less tight, easily exchangeable water molecules seem to occur at the lower ω_L values. Finally, the quadrupolar dips should specifically account for the behavior of protons bound the urethane N atoms.

In order to clarify and support these hypotheses, we considered the Inverse-Laplace transform curves of the relaxation kinetics data at five different ω_L values (namely 35, 10, 3, 1 and 0.3 MHz), obtained by means of the UPEN algorithm. Normalized transform curves (a representative example is shown in Figure 4) can be subjected to regression analysis as skewed log-normal distributions, the maximum and the full width ah half-height (fhmw) values of which were considered (Table 2, the complete dataset is reported in the Supporting Information, Table S3).

Table 2. Parameters for the Inverse-Laplace transforms (UPEN).

Sample	ω_L (MHz)	Max (ns)	fhmw (ns)	Pop. (%)	Sample	ω_L (MHz)	Max (ns)	fhmw (ns)	Pop. (%)
βCD	35	303	141	100	NS1 dry	35	142	47	100
	10	122	49	100		10	46	26	100
	3	36.2	12.1	100		3	10.7	2.8	100
	1	13.3	8.3	100		1	6.6	2.1	100
	0.3	5.1	1.8	100		0.3	2.8	0.7	100
NS2 dry	35	145	67	100	NS3 dry	35	234	62	100
	10	43	24	100		10	76	33	100
	3	9.5	3.8	100		3	16.3	7.3	100
	1	5.9	2.3	100		1	4.6	2.9	100
	0.3	2.5	1.2	100					
NS1+H_2O	35	770	319	80	NS2+H_2O	35	1442	1023	81
		231	205	20			129	117	19
	10	526	352	82		10	906	1164	83
		66	106	18			44	40	17
	3	394	461	84		3	860	1175	82
		19.0	22.6	16			11.2	16.0	18
	1	392	382	85		1	793	888	83
		13.2	12.9	15			9.9	11.7	17
	0.3	314	328	91		0.3	715	1003	86
		9.8	11.9	9			5.8	13.5	14
NS1+D_2O	35	160	124	100					
	10	734	714	37					
		52	52	63					
	3	14.3	32	100					
	1	210	226	9					
		10.6	14.6	91					
	0.3	179	274	21					
		3.0	7.1	79					

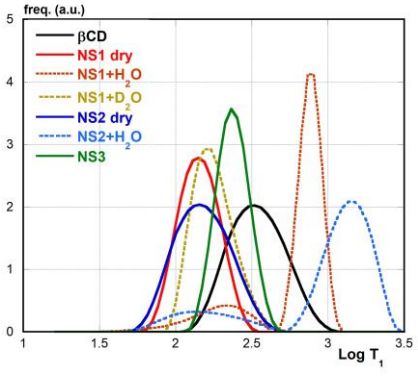

Figure 4. Normalized Inverse-Laplace transforms (UPEN) at 35 MHz.

As long as dry samples are concerned, all Inverse-Laplace transforms afford a unimodal distribution at any Larmor frequency, according to the observed first-order relaxation kinetics. Consistently with the discussion of dispersion curves reported hereinabove, the distributions maxima increase along the series NS2 ≈ NS1 < NS3 < βCD. This trend fairly agrees with the reticulation extent of the materials, but for the fact that values for NS1 are slightly larger than for NS2. The latter apparent anomaly might be justified with the much larger presence in NS1 of the hexamethylene linker chains, which benefit from a moderate conformational flexibility. Conversely, transforms for wet samples show bimodal distributions. Their major component is centered at larger T_1 values as compared to those found for dry materials, whereas the minor component is centered at comparable T_1 values. This finding, in turn, is consistent with the

occurrence of the complex relaxation kinetics observed in these cases. More in detail, the two components correspond to the slow and fast counterparts of the relaxation kinetics respectively. As long as the samples with H_2O are concerned, the two distribution maxima for NS1 occur at much lower T_1 values in comparison to NS2, consistently with its more extensive reticulation. On the other hand, maxima for the fast component occur at significantly larger values with respect to dry materials, accounting for larger molecular motions, which can be attributed to both the skeletal ^1H atoms and the hydration shell water molecules. The distribution maximum relevant to the fast component for the NS1+D_2O sample is in an intermediate position between the ones for dry NS1 and NS1+H_2O. The latter detail confirms the effect of swelling in increasing molecular motions for the skeletal H atoms in the wet sample.

Finally, the relative populations of the two components significantly change on varying the Larmor frequency. In particular, for NS1+H_2O the fast component passes from a 20% population at 35 MHz down to 9% at 0.3 MHz, whereas for NS2+H_2O, the fast component passes from 19% down to 14% population in the same ω_L range. The latter observations strongly support the idea that the sensitivity of the relaxometric response to water molecules tightly interacting with the nanosponge framework decreases on decreasing the Larmor frequency.

Texture features and Connectivity Indexes

At this point the question arises of how the relaxometric behavior observed may enable to gain information on the texture properties. According to theory,[54-56, 74] for wet micro- or nano-porous materials the relaxation rates R_1 can be related to the fraction of water molecules interacting with the pore surface (f_s) by the equation:

$$R_1 = R_w + f_s \cdot (R_s - R_w) \quad (3)$$

where R_w is the relaxation rate of bulk water (ca. 0.33 s^{-1},[55] almost independent on ω_L in the frequency range analyzed in this study) and R_s is the intrinsic relaxation rate for "surface" water. Hence, R_1 can lead back to the porosimetric parameters of the material according to the relationships:

$$R_1 = R_w + \rho \cdot (S/V) \quad (4)$$

$$R_1 = R_w + \rho \cdot (m/D) \quad (5)$$

$$R_1 = R_w + \lambda \cdot (m/D) \cdot (R_s - R_w) \quad (6)$$

where ρ is a parameter defined as the "surface relaxivity" (in the case of clay materials or natural soils, for instance, ρ values have been reported[55-56, 74] in the range of ca. 5~60 μm s^{-1}), λ represents the thickness of the hydration shell of pore walls (usually set as large as 0.3 nm) and m is a geometry parameter, the value of which is a function of pore shape (m = 4 for cylindrical pores, 6 for spherical ones). By comparing equations 3 and 6, it immediately follows: $D = \lambda \cdot m / f_s$.

In our case, assuming that the fast and slow components of the relaxation kinetics for wet samples adequately describe the behavior of surface and pore water molecules, respectively, according to the previous discussion, it can be obtained:

$$R_{slow} = R_w + f_s \cdot (R_{fast} - R_w) \quad (7)$$

and then:

$$f_s = (R_{slow} - R_w)/(R_{fast} - R_w) \quad (8)$$

Interestingly, the apparent values of f_s calculated from our data, vary as a function of ω_L (Figure 5, see data in the Supporting Information, Table S4), passing through a minimum located between 1 and 2 MHz. This implies that even the apparent thickness (λ) of the hydration shell of the pore surface depends on ω_L as well, according to the relationship: $\lambda = f_s \cdot (V/S)$ (which can be obtained combining equations 3-6), where the ratio V/S must be a constant, as an intrinsic feature of the material.

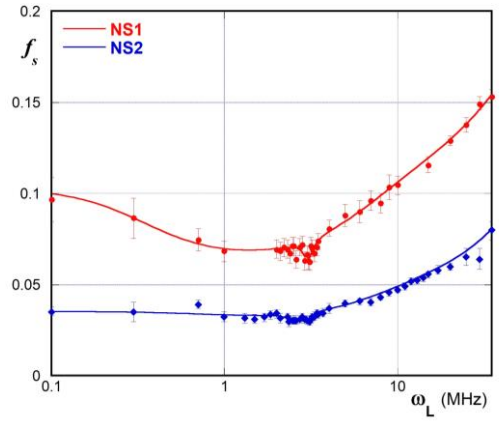

Figure 5. Apparent dependence of f_s on ω_L for NS1 and NS2.

We may reason that the value of 0.3 nm assumed for λ in the case of clays and soils, is conceivably unsuitable for nanosponges. In fact, water molecules can form clusters into the βCD cavities (0.78 nm). It is reasonable to assume that a similar behavior may be also shown by water molecules constrained into channels of similar width. Moreover, the secondary rim of cyclodextrins is able to exert a highly ordering effect on the water molecules located in its immediate surroundings, in such a way to form a so-called "expanded hydrophobic sphere".[75-77] The presence of this peculiar arrangement of water molecules is able to significantly affect the thermodynamics of binding of long-chain guests in solution. In particular, there is positive evidence that the size of the "expanded hydrophobic sphere" is roughly as large as an extended propylene diamine chain (i.e. ca. 0.5 nm).[78] Finally, the hydrophobic hexamethylene chains may induce an extensive clusterization of water molecules, due to the hydrophobic effect. This, in turn, affects the long-range solvent organization in the nearby. On the whole, consistently with the discussion of the R_1 vs ω_L curves reported hereinabove, our results can be rationalized assuming that the relaxometric response is able to sample at the largest ω_L values a long-range structuration of the pore solvent shell, that is somehow less perceived at the lowest ω_L values.

By considering equation 8, the average pore diameters of the materials may be related to relaxation rates according to the following expressions:

$$D = \lambda \cdot m / f_s =$$
$$= \lambda \cdot m \cdot (R_{fast} - R_w)/(R_{slow} - R_w) =$$
$$= \lambda \cdot m \cdot (1/T_{fast} - R_w)/(1/T_{slow} - R_w) \quad (9)$$

Unfortunately, based on the previous discussion, equation 9 cannot be applied in our case, because neither λ nor *m* values can be satisfactorily set. In particular, it is hardly possible to unambiguously define the pore-shape-depending *m* parameter, because of both the disordered NS microscopic structure and the unpredictable swelling effects. Nevertheless, it is interesting to notice that (as it can be easily verified from the data in Table S4) the ratio between the f_s values for NS1 and NS2 is independent of ω_L. More in detail, we found $f_{s,NS1}/f_{s,NS2} = 2.2 \pm 0.3$, which hence provides a reasonable estimation of the ratio between the average pore diameters for the two materials. Furthermore, the existence of a distribution of relaxation times, mirroring pore size distribution, must be considered. Indeed, the normalized Inverse-Laplace transforms provide a frequency distribution function ($P(T_1)$) for the T_1 values, so that we can define an average relaxation time $<T_1>$ as:

$$< T_1 > = \int_0^\infty P(T_1) T_1 dT_1 \qquad (10)$$

In order to apply equation 9, average values for T_{fast} and T_{slow} should be calculated according to equation 10, by considering independently the normalized fitting expressions for the fast and the slow components in place of $P(T_1)$. Noticeably, because *D* can be expressed as a function of T_{fast} and T_{slow} by equation 9, the normalized frequency distribution $P(T_1)$ for the isolated slow component may be transformed in a frequency distribution function for pore diameters ($P'(D)$) by a trivial variable exchange, i.e.:

$$P'(D) = P\left(\left[R_w + \frac{\lambda \cdot m}{D}\left(< T_{fast} >^{-1} - R_w\right)\right]\right) \qquad (11)$$

Then, the average pore size could be calculated as:

$$D = \int_0^\infty P'(D) D dD \qquad (12)$$

Once again, lack of reliable values for λ and *m* forbids defining the function $P'(D)$; so, even calculation of *D* according to equation 12 is not possible.

After having examined the intrinsic difficulties in assessing a satisfactory method to evaluate the textural parameters, we explored some alternative approaches. As we mentioned in the Introduction, soil properties have been adequately described, on the base of the relaxometric responses, by introducing the concept of "connectivity". In particular, two "connectivity indexes" have been defined: a "Functional Connectivity Index" (FCI) and a "Structural Connectivity Index" (SCI). Starting from the probability function $P(T_1)$ defined in equation 10, two arbitrary reference T_1 values (T_A and T_B) are chosen according to the conditions:

$$\int_0^{T_A} P(T_1) dT_1 = 0.01 \text{ and } \int_0^{T_B} P(T_1) dT_1 = 0.99 \qquad (13)$$

in such a way that the interval T_A-T_B comprises the most significant part (98%) of the T_1 values distribution, accounting for water molecules mobility. Then, the aforementioned connectivity indexes are simply defined as: FCI = T_B/T_A and SCI = $T_B - T_A$. It is worth stressing here that the key point in defining the "connectivity" is the fact that it provides an elegant and viable way to describe the functional role of water in mediating the transport phenomena through the channel network, and how this affects the overall interaction/exchange abilities of the soil system. It is immediately apparent that such a role is perfectly mirrored in NS materials.

In order to apply these ideas in our case, we preferred to adopt a slightly more restrictive significance criterion, keeping into account only a 95% of the overall ^{1}H population. Therefore, we defined T_A and T_B by fixing the upper integration limits in equations 13 at 0.025 and 0.975, respectively. Then, by analogy with equation 9, according to the relevant discussion reported hereinabove, we defined a further "Pore Connectivity Index" (PCI) as:

$$PCI = \frac{\left(\int_{T_{A,fast}}^{T_{B,fast}} P(T_{fast}) T_{fast} dT_{fast}\right)^{-1} - R_w}{\left(\int_{T_{A,slow}}^{T_{B,slow}} P(T_{slow}) T_{slow} dT_{slow}\right)^{-1} - R_w} \qquad (14)$$

The values of FCI, SCI and PCI calculated from the relaxometric data relevant to the wet samples, are collected in Table 3.

Table 3. FCI, SCI and PCI values for NS1 and NS2.

ω_L (MHz)	NS1			NS2		
	FCI	SCI	PCI	FCI	SCI	PCI
35	1.98	547	4.3	3.30	1713	13.1
10	2.98	652	6.2	7.05	2750	28.0
3	6.36	953	18.2	7.15	2132	69.3
1	5.25	595	27.7	5.98	1708	87.5
0.3	5.58	565	26.0	8.74	2088	46.4

At any Larmor frequency, the values of the three indexes are larger for NS2 than for NS1. This is perfectly consistent with the different reticulation extent. Neither FCI nor SCI show regular variations as a function of ω_L. This accords with the findings of a previous work on soils.[62] However, we can notice that FCI tends to decrease on increasing ω_L, whereas SCI may be considered roughly constant. Differently, PCI values for both materials pass through a maximum, centered at 1 MHz. Again, the ratio between the PCI values for the two materials does not depend on ω_L, within the reasonable statistical variations ($PCI_{NS2}/PCI_{NS1} = 3.2 \pm 0.6$). Therefore, PCI can be considered as a measure of the different mobility of water molecules within the nanochannels of the two different materials.

On the whole, these findings suggest that PCI can be considered an excellent alternative parameter (with respect to the textural *D*, *S* and *V* values), providing a satisfactory assessment of the textural features of nanosponges from a functional standpoint. In particular, PCI has the advantage to bypass the intrinsic difficulties deriving from the poor definition of the λ and *m*, the values of which critically depend on the highly disordered and swellable microscopic NS structure. Finally, in comparison with the previous FCI and SCI indexes, PCI benefits from the fact that its trend is independent of ω_L, thereby appearing easier to be rationalized.

CONCLUSIONS

This study reports for the first time the application of Fast-Field-Cycling NMR relaxometry, to gain information on the textural features of nanosponges. In particular, the study of wet samples revealed a complex behavior, which was attributed to the existence of two different water molecules populations, having significantly different relaxation rates and molecular mobility. This, in turn, led back to the pore size distribution in the materials. Moreover, inspired by the results from soil science, we adapted to nanosponges the concepts of connectivity indexes. Calculations performed by the Inverse-Laplace distributions revealed that a Pore Connectivity Index (PCI) can be suitably defined. Its values are positively related to the reticulation degree of the synthesized NSs.

As a final remark, even though the FFC relaxometric method does not allow to directly obtain the actual pore size distribution function, the PCI index provides a way to quantitatively assess the functional features of nanosponges. This, in turn, may be a valuable tool for rationalizing the supramolecular behavior and abilities of these materials. Thus, it may be helpful for clarifying the molecular mechanisms involved in their controlled absorption and release properties, and, in perspective, for a rationale design of tailored systems.

ASSOCIATED CONTENT

Supporting Information. *i*) Short outline of FFC-NMR theory; *ii*) Synthesis of NSs; *iii*) Instrumentation; *iv*) **Table S1**. R_1 vs ω_L data; *v*) **Table S2**. Halle's regression parameters R_1 vs ω_L curves; *vi*) **Table S3**. Log-normal regression parameters for Inverse-Laplace (UPEN) T_1 distribution curves; *vii*) **Table S4**. f_s vs ω_L data for NS1 and NS2. This material is available free of charge via the Internet at http://pubs.acs.org.

AUTHOR INFORMATION

Corresponding Authors

* paolo.lomeo@unipa.it
* pellegrino.conte@unipa.it

Author Contributions

All authors have given approval to the final version of the manuscript.

Funding Sources

University of Palermo (FFR funding) is gratefully acknowledged for financial support.

ACKNOWLEDGMENT

Prof. G. Lazzara and Dr. S. Cataldo (Dept. of Physics and Chemistry, University of Palermo) are gratefully acknowledged for TGA determinations. Prof. M.L. Saladino and Dr. G. Polito (Dept. STEBICEF, University of Palermo) are gratefully acknowledged for BET/BJH measurements.

ABBREVIATIONS

BET: Braunauer-Emmett-Teller theory; BJH: Barrett-Joyner-Halenda theory; FFC: Fast-Field-Cycling.

REFERENCES

1. Caldera, F.; Tannous, M.; Cavalli, R.; Zanetti, M.; Trotta, F., Evolution of Cyclodextrin Nanosponges. *Int. J. Pharm.* **2017,** *531* (2), 470-479.
2. *Nanosponges: Synthesis and Applications*. Trotta, F., Mele. A., Eds.; Wiley-VCH Verlag GmbH & Co. KGaA: Weinheim, Germany, **2019**.
3. Pawar, S.; Shende, P.; Trotta, F., Diversity of β-cyclodextrin-based nanosponges for transformation of actives. *Int. J. Pharm.* **2019,** *565*, 333-350.
4. Sherje, A. P.; Dravyakar, B. R.; Kadam, D.; Jadhav, M., Cyclodextrin-based nanosponges: A critical review. *Carbohydr. Polym.* **2017,** *173*, 37-49.
5. Taka, A. L.; Fosso-Kankeu, E.; Pillay, K.; Mbianda, X. Y., Removal of cobalt and lead ions from wastewater samples using an insoluble nanosponge biopolymer composite: adsorption isotherm, kinetic, thermodynamic, and regeneration studies. *Environmental Science and Pollution Research* **2018,** *25* (22), 21752-21767.
6. Fontana, R. M.; Milano, N.; Barbara, L.; Di Vincenzo, A.; Gallo, G.; Lo Meo, P., Cyclodextrin-Calixarene Nanosponges as Potential Platforms for pH-Dependent Delivery of Tetracycline. *ChemistrySelect* **2019,** *4* (33), 9743-9747.
7. Allahyari, S.; Trotta, F.; Valizadeh, H.; Jelvehgari, M.; Zakeri-Milani, P., Cyclodextrin-based nanosponges as promising carriers for active agents. *Expert Opin. Drug Del.* **2019,** *16* (5), 467-479.
8. Sikder, M. T.; Rahman, M. M.; Jakariya, M.; Hosokawa, T.; Kurasaki, M.; Saito, T., Remediation of water pollution with native cyclodextrins and modified cyclodextrins: A comparative overview and perspectives. *Chem. Eng. J.* **2019,** *355*, 920-941.
9. Morin-Crini, N.; Winterton, P.; Fourmentin, S.; Wilson, L. D.; Fenyvesi, É.; Crini, G., Water-insoluble β-cyclodextrin–epichlorohydrin polymers for removal of pollutants from aqueous solutions by sorption processes using batch studies: A review of inclusion mechanisms. *Prog. Polym. Sci.* **2018,** *78*, 1-23.
10. Russo, M.; Spinella, A.; Di Vincenzo, A.; Lazzara, G.; Correro, M. R.; Shahgaldian, P.; Lo Meo, P.; Caponetti, E., Synergistic Activity of Silver Nanoparticles and Polyaminocyclodextrins in Nanosponge Architectures. *ChemistrySelect* **2019,** *4* (3), 873-879.
11. Sadjadi, S.; Heravi, M. M.; Malmir, M., Pd(0) nanoparticle immobilized on cyclodextrin-nanosponge-decorated Fe2O3@SiO2 core-shell hollow sphere: An efficient catalyst for C–C coupling reactions. *J. Taiwan Inst. Chem. Eng.* **2018,** *86*, 240-251.
12. Martin-Trasanco, R.; Cao, R.; Esparza-Ponce, H. E.; Montero-Cabrera, M. E.; Arratia-Pérez, R., Reduction of Au(III) by a β-cyclodextrin polymer in acid medium. A stated unattainable reaction. *Carbohydr. Polym.* **2017,** *175*, 530-537.
13. Vasconcelos, D. A.; Kubota, T.; Santos, D. C.; Araujo, M. V. G.; Teixeira, Z.; Gimenez, I. F., Preparation of Au_n quantum clusters with catalytic activity in β-cyclodextrin polyurethane nanosponges. *Carbohydr. Polym.* **2016,** *136*, 54-62.
14. Trotta, F., Cyclodextrin Nanosponges and their Applications. In *Cyclodextrins in Pharmaceutics, Cosmetics, and Biomedicine*, pp 323-342. Bilensoy, E., Ed.; John Wiley & Sons, Inc., Hoboken, NJ, **2011**.
15. Spinella, A.; Russo, M.; Di Vincenzo, A.; Chillura Martino, D.; Lo Meo, P., Hyper-reticulated calixarene polymers: a new example of entirely synthetic nanosponge materials. *Beilstein J. Org. Chem.* **2018,** *14*, 1498-1507.
16. Lu, P.; Cheng, J.; Li, Y.; Li, L.; Wang, Q.; He, C., Novel porous β-cyclodextrin/pillar[5]arene copolymer for rapid removal of organic pollutants from water. *Carbohydr. Polym.* **2019,** *216*, 149-156.

17. Cinà, V.; Russo, M.; Lazzara, G.; Chillura Martino, D.; Lo Meo, P., Pre- and post-modification of mixed cyclodextrin-calixarene co-polymers: A route towards tunability. *Carbohydr. Polym.* **2017,** *157*, 1393-1403.

18. Russo, M.; Saladino, M. L.; Chillura Martino, D.; Lo Meo, P.; Noto, R., Polyaminocyclodextrin nanosponges: Synthesis, characterization and pH-responsive sequestration abilities. *RSC Adv.* **2016,** *6* (55), 49941-49953.

19. Di Vincenzo, A.; Russo, M.; Cataldo, S.; Milea, D.; Pettignano, A.; Lo Meo, P., Effect of pH Variations on the Properties of Cyclodextrin-Calixarene Nanosponges. *ChemistrySelect* **2019,** *4* (20), 6155-6161.

20. Castiglione, F.; Crupi, V.; Majolino, D.; Mele, A.; Rossi, B.; Trotta, F.; Venuti, V., Effect of cross-linking properties on the vibrational dynamics of cyclodextrins-based polymers: An experimental-numerical study. *J. Phys. Chem. B* **2012,** *116* (27), 7952-7958.

21. Crupi, V.; Fontana, A.; Giarola, M.; Longeville, S.; Majolino, D.; Mariotto, G.; Mele, A.; Paciaroni, A.; Rossi, B.; Trotta, F.; Venuti, V., Vibrational density of states and elastic properties of cross-linked polymers: Combining inelastic light and neutron scattering. *J. Phys. Chem. B* **2014,** *118* (2), 624-633.

22. Trotta, F.; Caldera, F.; Dianzani, C.; Argenziano, M.; Barrera, G.; Cavalli, R., Glutathione Bioresponsive Cyclodextrin Nanosponges. *ChemPlusChem* **2016,** *81* (5), 439-443.

23. Brunauer, S.; Emmett, P. H.; Teller, E., Adsorption of Gases in Multimolecular Layers. *J. Am. Chem. Soc.* **1938,** *60* (2), 309-319.

24. Kruk, M.; Antochshuk, V.; Jaroniec, M.; Sayari, A., New Approach to Evaluate Pore Size Distributions and Surface Areas for Hydrophobic Mesoporous Solids. *J. Phys. Chem. B* **1999,** *103* (48), 10670-10678.

25. Alsbaiee, A.; Smith, B. J.; Xiao, L. L.; Ling, Y. H.; Helbling, D. E.; Dichtel, W. R., Rapid removal of organic micropollutants from water by a porous beta-cyclodextrin polymer. *Nature* **2016,** *529* (7585), 190-U146.

26. Li, Y.; Lu, P.; Cheng, J.; Zhu, X.; Guo, W.; Liu, L.; Wang, Q.; He, C.; Liu, S., Novel microporous β-cyclodextrin polymer as sorbent for solid-phase extraction of bisphenols in water samples and orange juice. *Talanta* **2018,** *187*, 207-215.

27. Li, H.; Meng, B.; Chai, S.-H.; Liu, H.; Dai, S., Hyper-crosslinked β-cyclodextrin porous polymer: an adsorption-facilitated molecular catalyst support for transformation of water-soluble aromatic molecules. *Chem. Sci.* **2016,** *7* (2), 905-909.

28. Xiao, P.; Dudal, Y.; Corvini, P. F. X.; Shahgaldian, P., Polymeric cyclodextrin-based nanoparticles: Synthesis, characterization and sorption properties of three selected pharmaceutically active ingredients. *Polym. Chem.* **2011,** *2* (1), 120-125.

29. Wilson, L. D.; Mohamed, M. H.; Berhaut, C. L., Sorption of aromatic compounds with copolymer sorbent materials containing β-cyclodextrin. *Materials* **2011,** *4* (9), 1528-1542.

30. Pratt, D. Y.; Wilson, L. D.; Kozinski, J. A.; Mohart, A. M., Preparation and sorption studies of β-cyclodextrin/epichlorohydrin copolymers. *J. Appl. Polym. Sci.* **2010,** *116* (5), 2982-2989.

31. Gholibegloo, E.; Mortezazadeh, T.; Salehian, F.; Ramazani, A.; Amanlou, M.; Khoobi, M., Improved curcumin loading, release, solubility and toxicity by tuning the molar ratio of cross-linker to β-cyclodextrin. *Carbohydr. Polym.* **2019,** *213*, 70-78.

32. Junthip, J.; Promma, W.; Sonsupap, S.; Boonyanusith, C., Adsorption of paraquat from water by insoluble cyclodextrin polymer crosslinked with 1,2,3,4-butanetetracarboxylic acid. *Iranian Polymer Journal (English Edition)* **2019,** *28* (3), 213-223.

33. Junthip, J., Water-insoluble cyclodextrin polymer crosslinked with citric acid for paraquat removal from water. *J. Macromol. Sci., Part A: Pure Appl.Chem.* **2019,** *56* (6), 555-563.

34. Lo Meo, P.; Lazzara, G.; Liotta, L.; Riela, S.; Noto, R., Cyclodextrin-calixarene co-polymers as a new class of nanosponges. *Polym. Chem.* **2014,** *5* (15), 4499-4510.

35. Wilson, L. D.; Mohamed, M. H.; Headley, J. V., Surface area and pore structure properties of urethane-based copolymers containing β-cyclodextrin. *J. Colloid Interf. Sci.* **2011,** *357* (1), 215-222.

36. Brownstein, K. R.; Tarr, C. E., Relaxation time versus water content: Linear or nonlinear? *Science* **1976,** *194* (4261), 213-214.

37. Brownstein, K. R.; Tarr, C. E., Spin-lattice relaxation in a system governed by diffusion. *Journal of Magnetic Resonance (1969)* **1977,** *26* (1), 17-24.

38. Brownstein, K. R.; Tarr, C. E., Importance of classical diffusion in NMR studies of water in biological cells. *Physical Review A* **1979,** *19* (6), 2446-2453.

39. Mattea, C.; Fatkullin, N.; Fischer, E.; Beginn, U.; Anoardo, E.; Kroutieva, M.; Kimmich, R., The "corset effect" of spin-lattice relaxation in polymer melts confined in nanoporous media. *Appl. Magn. Reson.* **2004,** *27* (3), 371-381.

40. Phani Kumar, B. V. N.; Stapf, S.; Mattea, C., Molecular Dynamics in the Lyophases of Copolymer P123 Investigated with FFC NMR Relaxometry. *Langmuir* **2019,** *35* (2), 435-445.

41. Ferrante, G.; Sykora, S., Technical aspects of Fast Field Cycling. In *Adv. Inorg. Chem.*, **2005**; Vol. 57, pp 405-470.

42. Kruk, D.; Herrmann, A.; Rössler, E. A., Field-cycling NMR relaxometry of viscous liquids and polymers. *Prog. Nucl. Magn. Reson. Spectrosc.* **2012,** *63*, 33-64.

43. Rössler, E. A.; Stapf, S.; Fatkullin, N., Recent NMR investigations on molecular dynamics of polymer melts in bulk and in confinement. *Curr. Opin. Colloid Interface Sci.* **2013,** *18* (3), 173-182.

44. Flämig, M.; Hofmann, M.; Lichtinger, A.; Rössler, E. A., Application of proton field-cycling NMR relaxometry for studying translational diffusion in simple liquids and polymer melts. *Magn. Reson. Chem.* **2019,** *57* (10), 805-817.

45. Parigi, G.; Rezaei-Ghaleh, N.; Giachetti, A.; Becker, S.; Fernandez, C.; Blackledge, M.; Griesinger, C.; Zweckstetter, M.; Luchinat, C., Long-Range Correlated Dynamics in Intrinsically Disordered Proteins. *J. Am. Chem. Soc.* **2014,** *136* (46), 16201-16209.

46. Di Gregorio, E.; Ferrauto, G.; Lanzardo, S.; Gianolio, E.; Aime, S., Use of FCC-NMRD relaxometry for early detection and characterization of ex-vivo murine breast cancer. *Scientific reports* **2019,** *9* (1), 4624.

47. Steele, R. M.; Korb, J. P.; Ferrante, G.; Bubici, S., New applications and perspectives of fast field cycling NMR relaxometry. *Magn. Reson. Chem.* **2016,** *54* (6), 502-509.

48. Araya, Y. T.; Martínez-Santiesteban, F.; Handler, W. B.; Harris, C. T.; Chronik, B. A.; Scholl, T. J., Nuclear magnetic relaxation dispersion of murine tissue for development of T1 (R1) dispersion contrast imaging. *NMR Biomed.* **2017,** *30* (12).

49. Davies, S.; Packer, K. J.; Roberts, D. R.; Zelaya, F. O., Pore-size distributions from NMR spin-lattice relaxation data. *Magn. Reson. Imaging* **1991,** *9* (5), 681-685.

50. Korb, J. P.; Whaley Hodges, M.; Bryant, R., Translational diffusion of liquids at surface of microporous materials: New theoretical analysis of field cycling magnetic relaxation measurements. *Magn. Reson. Imaging* **1998,** *16* (5-6), 575-578.

51. Howard, J. J., Quantitative estimates of porous media wettability from proton NMR measurements. *Magn. Reson. Imaging* **1998,** *16* (5), 529-533.

52. Todoruk, T. R.; Langford, C. H.; Kantzas, A., Pore-Scale Redistribution of Water during Wetting of Air-Dried Soils As Studied by Low-Field NMR Relaxometry. *Environ. Sci. Technol.* **2003,** *37* (12), 2707-2713.

53. Mikutta, C.; Lang, F.; Kaupenjohann, M., Soil Organic Matter Clogs Mineral Pores. *Soil Sci. Soc. Am. J.* **2004,** *68* (6), 1853-1862.

54. Bird, N. R. A.; Preston, A. R.; Randall, E. W.; Whalley, W. R.; Whitmore, A. P., Measurement of the size distribution of water-filled pores at different matric potentials by stray field nuclear magnetic resonance. *Eur. J. Soil Sci* **2005,** *56* (1), 135-143.

55. Hinedi, Z. R.; Chang, A. C.; Anderson, M. A.; Borchardt, D. B., Quantification of microporosity by nuclear magnetic resonance relaxation of water imbibed in porous media. *Water Resour. Res.* **1997,** *33* (12), 2697-2704.

56. Pohlmeier, A.; Haber-Pohlmeier, S.; Stapf, S., A fast field cycling nuclear magnetic resonance relaxometry study of natural soils. *Vadose Zone J.* **2009,** *8* (3), 735-742.

57. Belorizky, E.; Fries, P. H.; Guillermo, A.; Poncelet, O., Almost ideal 1d water diffusion in imogolite nanotubes evidenced by NMR relaxometry. *ChemPhysChem* **2010,** *11* (9), 2021-2026.

58. Fleury, M.; Kohler, E.; Norrant, F.; Gautier, S.; M'Hamdi, J.; Barré, L., Characterization and Quantification of Water in Smectites with Low-Field NMR. *J. Phys. Chem. C* **2013,** *117* (9), 4551-4560.

59. Buchmann, C.; Bentz, J.; Schaumann, G. E., Intrinsic and model polymer hydrogel-induced soil structural stability of a silty sand soil as affected by soil moisture dynamics. *Soil Tillage Res.* **2015,** *154*, 22-33.

60. Conte, P., Chapter 10 Environmental Applications of Fast Field-cycling NMR Relaxometry. In *Field-cycling NMR Relaxometry: Instrumentation, Model Theories and Applications,* The Royal Society of Chemistry: **2019**; pp 229-254.

61. Conte, P.; Alonzo, G., Environmental NMR: Fast-field-cycling relaxometry. In *eMagRes,* **2013**; Vol. 2, pp 389-398.

62. Conte, P.; Ferro, V., Standardizing the use of fast-field cycling NMR relaxometry for measuring hydrological connectivity inside the soil. *Magn. Reson. Chem.* **2019**;1-10. https://doi.org/10.1002/mrc.4907.

63. Conte, P.; Ferro, V., Measuring hydrological connectivity inside a soil by low field nuclear magnetic resonance relaxometry. *Hydrol. Processes* **2018,** *32* (1), 93-101.

64. Kazuo, M.; Akio, K.; Yoshihisa, M.; Yoshio, D., Effects of Inorganic Salts on the Dissociation of a Complex of β-Cyclodextrin with an Azo Dye in an Aqueous Solution. *Bull. Chem. Soc. Jpn.* **1973,** *46* (12), 3703-3707.

65. Al Omari, M. M.; El-Barghouthi, M. I.; Zughul, M. B.; Davies, J. E. D.; Badwan, A. A., Dipyridamole/β-cyclodextrin complexation: effect of buffer species, thermodynamics, and guest–host interactions probed by 1H-NMR and molecular modeling studies. *J. Incl. Phenom. Macrocycl. Chem.* **2009,** *64* (3), 305-315.

66. Ghosh, M.; Zhang, R.; Lawler, R. G.; Seto, C. T., The Effects of Buffers on the Thermodynamics and Kinetics of Binding between Positively-Charged Cyclodextrins and Phosphate Ester Guests. *J. Org. Chem.* **2000,** *65* (3), 735-741.

67. Lo Meo, P.; D'Anna, F.; Gruttadauria, M.; Riela, S.; Noto, R., Binding properties of mono-(6-deoxy-6-amino)-β-cyclodextrin towards p-nitroaniline derivatives: a polarimetric study. *Tetrahedron* **2009,** *65* (50), 10413-10417.

68. Lo Meo, P.; D'Anna, F.; Riela, S.; Gruttadauria, M.; Noto, R., Spectrophotometric determination of binding constants between some aminocyclodextrins and nitrobenzene derivatives at various pH values. *Tetrahedron* **2002,** *58* (30), 6039-6045.

69. Russo, M.; La Corte, D.; Pisciotta, A.; Riela, S.; Alduina, R.; Lo Meo, P., Binding abilities of polyaminocyclodextrins: polarimetric investigations and biological assays. *Beilstein J. Org. Chem.* **2017,** *13*, 2751-2763.

70. Lo Meo, P.; D'Anna, F.; Riela, S.; Gruttadauria, M.; Noto, R., Binding equilibria between β-cyclodextrin and p-nitro-aniline derivatives: the first systematic study in mixed water-methanol solvent systems. *Tetrahedron* **2009,** *65* (10), 2037-2042.

71. Halle, B.; Jóhannesson, H.; Venu, K., Model-Free Analysis of Stretched Relaxation Dispersions. *Journal of Magnetic Resonance* **1998,** *135* (1), 1-13.

72. Halle, B., The physical basis of model-free analysis of NMR relaxation data from proteins and complex fluids. *J. Chem. Phys.* **2009,** *131* (22), 224507.

73. Bertini, I.; Fragai, M.; Luchinat, C.; Parigi, G., H NMRD profiles of diamagnetic proteins: A model-free analysis. *Magn. Reson. Chem.* **2000,** *38* (7), 543-550.

74. Stingaciu, L. R.; Weihermüller, L.; Haber-Pohlmeier, S.; Stapf, S.; Vereecken, H.; Pohlmeier, A., Determination of pore size distribution and hydraulic properties using nuclear magnetic resonance relaxometry: A comparative study of laboratory methods. *Water Resour. Res.* **2010,** *46* (11).

75. Rekharsky, M. V.; Inoue, Y., Complexation Thermodynamics of Cyclodextrins. *Chem. Rev.* **1998,** *98* (5), 1875-1918.

76. Matsui, Y.; Mochida, K., Binding Forces Contributing to the Association of Cyclodextrin with Alcohol in an Aqueous Solution. *Bull. Chem. Soc. Jpn.* **1979,** *52* (10), 2808-2814.

77. Saenger, W., Cyclodextrin Inclusion Compounds in Research and Industry. *Angew. Chem. Int. Ed. Eng.* **1980,** *19* (5), 344-362.

78. Lo Meo, P.; D'Anna, F.; Gruttadauria, M.; Riela, S.; Noto, R., Thermodynamics of binding between α- and β-cyclodextrins and some p-nitro-aniline derivatives: reconsidering the enthalpy–entropy compensation effect. *Tetrahedron* **2004,** *60* (41), 9099-9111.

Insert Table of Contents artwork here